JOURNAL OF MATERIALS SCIENCE 28 (1993) 4518–4529

Nuclear track method for neutron-induced radionuclide mapping with applications to uranium distributions in superconductors

R. L. FLEISCHER*
General Electric Research and Development Center, Schenectady, NY 12301, USA

Intermetallic and oxide superconductors can be improved by internal heavy ion irradiation damage produced by doping the materials with uranium followed by neutron-induced fission. The uniformity or the scale of the lack of it in the uranium distribution is critical to whether the superconducting phase is uniformly irradiated and the effect optimized. In this work we describe, first, how one can measure the distribution and, second, what it is in recently tested Y–Ba–Cu and Bi–Pb–Sr–Ca–Cu oxide superconductors. The bulk of this work is a primarily tutorial description of the solid-state-track detector method, concentrating on optimizing spatial resolution. It reviews existing work, emphasizing examples of doped intermetallic superconductors; it also includes some new quantitative aspects of the technique. The second part gives results from using these techniques on oxide superconductors, for which the resolution is pushed to its limits. Nevertheless, it is good enough to conclude that in Y–Ba–Cu–O the uranium is mostly within the superconducting phase. In Bi–Pb–Ca–Sr–O it can be said only that the uranium is not primarily in minor phases. Resolution in that material is such that the uranium could either uniformly coat grains or lie within them.

1. Introduction

Irradiation damage can improve the current-carrying capacity of superconductors by introducing defects or clusters of defects that impede the motion of magnetic flux lines. The first type of irradiation to be tested was by fast neutrons, originally [1–3] for intermetallic "high-temperature" superconductors, such as [2] V_3Si, V_3Ga, Nb_3Al and Nb_3Sn and in other studies [1, 3] NbZr and Nb_3Sn; more recently neutron irradiation has been applied to oxide superconductors [4–6].

A more concentrated form of irradiation (in the sense of clustering atomic defects) can be provided by heavy ions. Although penetrating beams of heavy ions are available at a few major accelerators, beam time is in demand, and it is difficult and inconvenient to obtain uniform irradiations over sizable volumes of material. A potentially simpler means of producing spatially uniform radiation damage by heavy ions is to disperse fissionable atoms, such as ^{235}U or ^{239}Pu [or those that undergo (n, α) reactions, such as ^{10}B or ^{6}Li], within the superconductor and induce fission with thermal neutrons. The major fission energy is in a pair of heavy ions for each fission, ions that typically travel $\sim 10\ \mu m$ in opposite directions from the site of the fissioned nucleus. Such internal irradiations have been shown to be highly effective in improving the current-carrying properties of the intermetallics [7–9] Nb_3Al, V_3Si and Nb_3Sn and in the oxide superconductors [10–13] of Y–Ba–Cu and Bi–Pb–Sr–Ca–Cu doped with uranium; in one study [7] boron doping and irradiation was used.

1.1. Dispersion of fissionable elements

The distribution of uranium is critical to optimizing its effect. Minor concentrations of uranium in solids can be dispersed uniformly, as is typically true in glass [14], or highly non-uniformly, as seen in poly-phase material [15]. Fig. 1 sketches possible distributions. If the uranium lies primarily in a minor phase or in grain boundaries, the fission fragments may fail to reach the full volume of the material, the decisive factor being the scale of the dispersion relative to the range R of the fission fragments. If uranium were solely in the grain boundaries and the grain size d was much larger than R, only the near-surface portions of the grains would be irradiated. For $d < R$ it is unimportant whether the uranium is uniform volumetrically or spread on grain boundaries. It is also possible that a minority phase contains a majority of the uranium [15]. In such a case the distribution of the second phase may only allow a minute fraction of the major conducting phase to be irradiated by fission fragments. If so, the doping-plus-irradiation would be ineffective.

Although doping and irradiation were effective in the superconducting oxides, in the work referenced

* *Present address*: Renssealer Polytechnic Institute, Troy, NY 12180-3590, USA.

0022–2461

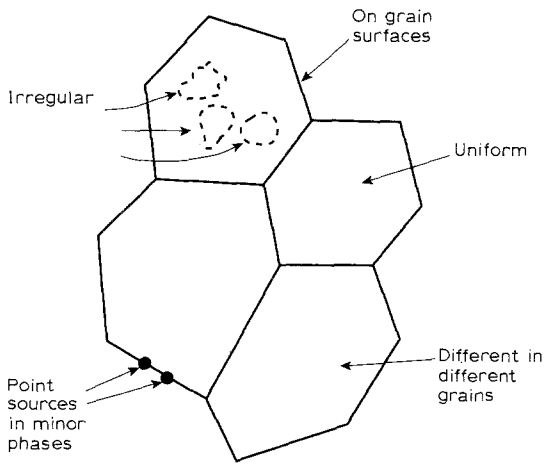

Figure 1 Hypothetical uranium distributions in a polycrystalline solid. The blotchy distribution would arise if equilibrium was not obtained. Grain boundary segregation could arise from low solubility in the crystalline phases.

[10–13] d was not very different from R. By measuring the uranium distributions in those samples it might be possible to decide whether the same desirable effect could still be attained once improvements in processing allow samples of larger grain size to be prepared.

The technique used—fission autoradiography—allows uranium distributions to be mapped in a material by first placing a solid state track detector (such as muscovite mica) against a sample of interest (see sketches in Fig. 2), then using thermal neutrons to induce fission, and later revealing the tracks in the detector by preferential chemical etching [16]. The mapping technique was devised by Price and Walker [17] in 1963 and is elaborated in reference [16]. With thick samples and conventional use the resolution is comparable with the particle range R. Since in the present case $d \sim R$, improvements in resolution are used. The main purpose of this work is to review briefly the applications of the nuclear track technique for observing uranium distributions and to describe techniques for enhancing resolution.

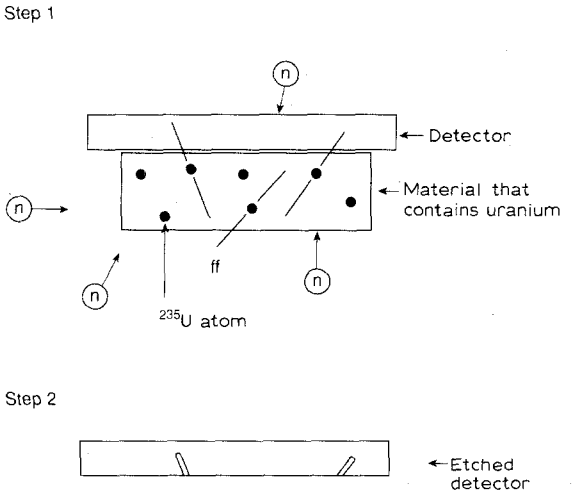

Figure 2 Fission radiography allows uranium to be measured and its distribution to be mapped in a detector placed against a sample. Fission is induced by thermal neutrons. Tracks are later revealed by chemical etching.

2. Uranium measurement technique

2.1. Uranium concentration

For the method sketched in Fig. 2 the fission fragment density ρ_f (per cm^2) that enters the detector is given by

$$\rho_f = \sigma\phi N_v I c R/2 \qquad (1)$$

where σ = thermal neutron cross-section for ^{235}U, ϕ = thermal neutron dose, N_v = number of atoms per cm^3 of sample, I = isotopic abundance of ^{235}U (0.00719), c = atom fraction of uranium in the sample and R = average fission fragment range in the sample.

The density of tracks ρ revealed by etching may be reduced from ρ_f by either of two factors, an etching efficiency η if it is less than unity and (R_r/R_d) where R_r is a reduced range in the detector for the case where the full trajectory of the ions in the detector is not revealed by etching. R_d is the full range in the detector. For the mica used here $\eta = 1$, $R_d = 12.2\,\mu m$, $R_r = 10.8\,\mu m$, and hence $R_r/R_d = 0.88$ [18, 19]. The uranium concentration may either be calculated from c in Equation 1 or by reference to the track counts in a detector placed against a standard material of known uranium content [16, Chapter 8].

The procedure just described has remarkable sensitivity (to less than 10^{-5} wt parts million [20]) and gives reliable absolute values for thick samples with no intervening matter between sample and detector. For samples that are thinner than R or those with intervening matter, the usual uncertainties in those thicknesses make the measured values of c much less precise. Adaptations of Equation 1 to such a case will be described later. As we shall see, however, such geometries may help in the main purpose here of observing spatial variations in c.

2.2. Mapping the variability of uranium

In addition to its high sensitivity, the other special merit of the track method is its ability to display elemental distributions. Fig. 3 shows that there is no ambiguity as to the location of a single uranium-rich dust particle on a mica detector [17]. Figs 4 and 5 show distributions in A15-structure intermetallic superconductors: blotchy, non-uniform boron distributions [7] in Nb_3Al and apparently uniform uranium distributions in the Nb_3Sn and Sn layers on Nb wires that were taper-sectioned [9]. The variations of uranium shown in these two photos are on scales that are large relative to track lengths, and therefore the distributions are clear. At the other extreme, Fig. 3 shows that isolated point sources are also clearly displayed, but they would be hard to distinguish if there were many with a spacing that is much less than typical track lengths.

To establish the resolution of a sharp boundary between regions where fission fragments are emitted and where they are not, the simple experiment shown in Fig. 6 was done. A layer of Pb overlying a thin ^{252}Cf source of fission fragments blocks all ions except those that cross the open space and cut a thin portion of the corner of the Pb. Fig. 7 shows the result, a relatively sharp demarkation apparently fuzzed over a region of

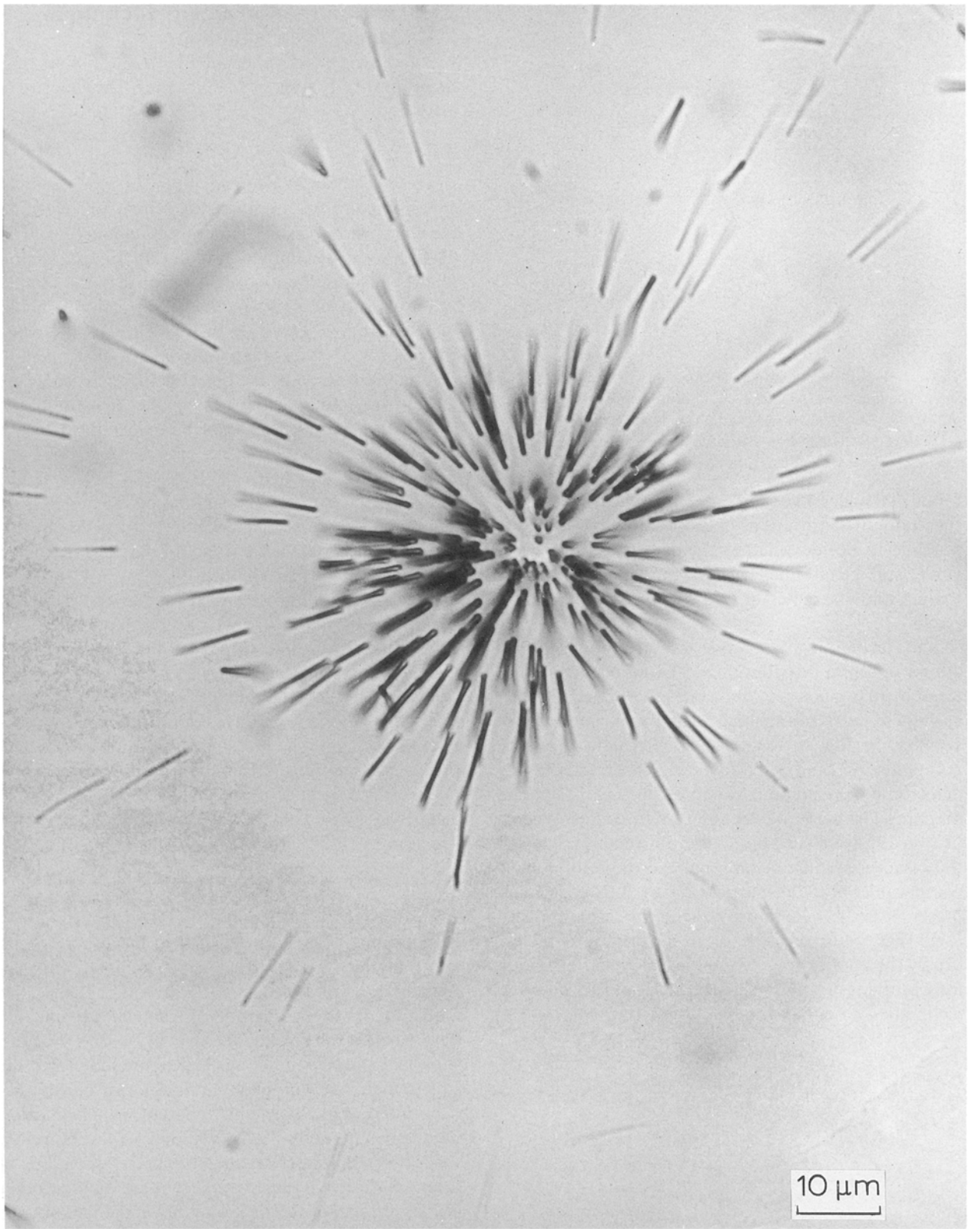

Figure 3 Fission tracks in a mica sample from a uranium-rich dust particle [17].

5–10 μm width. The cutoff will appear sharper if one views only the holes at the surface through which the fission fragments entered. The visibility of the full etched length blurs the boundary in a way that can be cured. It is helpful to know what is observed if contact between the lead and the detector is imperfect. In this case fission fragments can enter a gap between absorber and detector, and the boundary is compromised—as Fig. 8 makes clear. The gradient in track density extends over several tens of micrometres. Clearly, sample and detector must have snug contacts for best resolution.

What variation in the track density is expected from abrupt changes in uranium concentration? If one concentrates on the points of entry to the detector, the density as a function of distance y_0 from abrupt

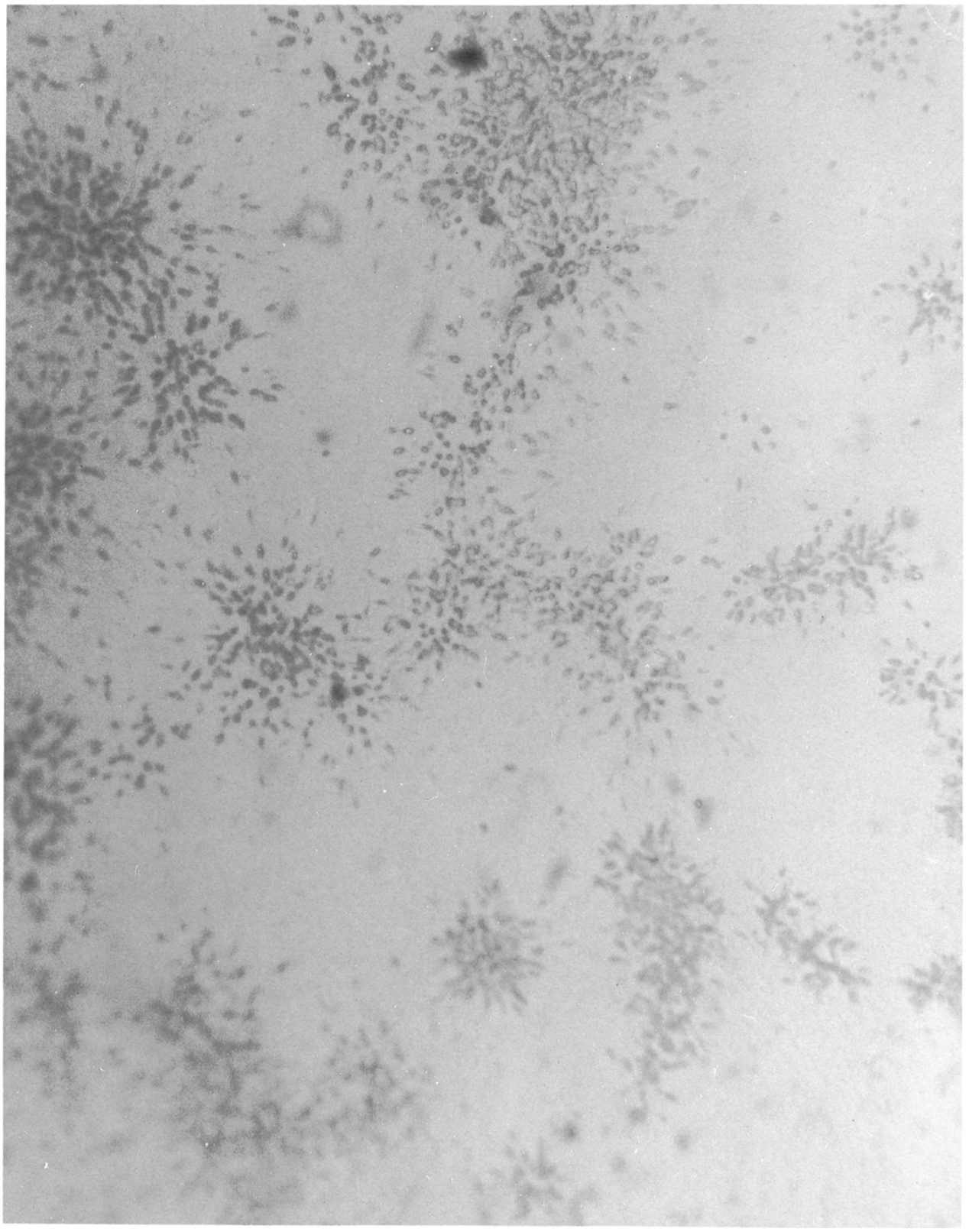

Figure 4 Boron distribution in Nb_3Al displayed by recording the ^4He and ^7Li particles from ^{10}B (n, α) reactions [7].

changes (such as the two that are shown in Fig. 9) is calculated by integrating over the volume that contains uranium and is also within a distance R of the position of interest

$$\rho = 2N_v \int_{y_0}^{R} \frac{\sin \phi \, dV}{4\pi r^2} \quad (2)$$

The quantities ϕ, y_0 and R in Equation 2 are defined in Fig. 10. The calculated ρ is for tracks from particles that cross the x–y plane at the origin in Fig. 10. The results are in Fig. 11. Across an abrupt change the track density goes from 0.7 to 0.2 of the maximum—a clearly recognizable change—over a distance of 0.35 R, i.e. about 3–4 μm. And at a planar distribution of uranium the width from 0.2 of the maximum to 0.2 of the maximum on the other side is ~ 2 μm. Hence, uranium that is concentrated at grain boundaries should be clearly imaged.

Figure 5 Uranium distribution in taper-sectioned Nb–Nb_3Sn–Sn wires. Uranium is confined to the two outer layers, Sn and Nb_3Sn.

Contrast enhancement: how does one view the points of entry into the detector, rather than the full tracks that are photographed in Figs 7 and 8? The simplest microscopic procedure is to use reflected light and focus on the entrances to the etched holes. Contrast is, however, often not optimal. Seitz, *et al.* [21] devised a superior technique, sketched in Fig. 12. Oblique shadowing with Ag or Al coats the detector with an opaque layer but does not fill the holes. Illumination from below shows the surface location of each track as an easily visible bright dot on a dark background. As an example, Fig. 13 shows the same general area as Fig. 7.

Even though the resolution ($\sim 4\ \mu m$) implied by the results in Fig. 11 is reasonably good, for 10 μm diameter grains $\pm 4\ \mu m$ on opposite sides means the

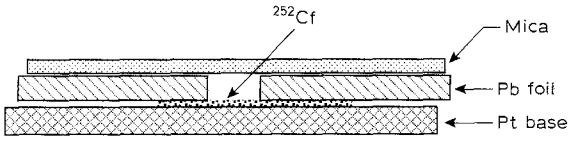

Figure 6 Control experiment to show edge resolution. ^{252}Cf spontaneously emits fission fragments. The lead foil stops all fragments at normal incidence.

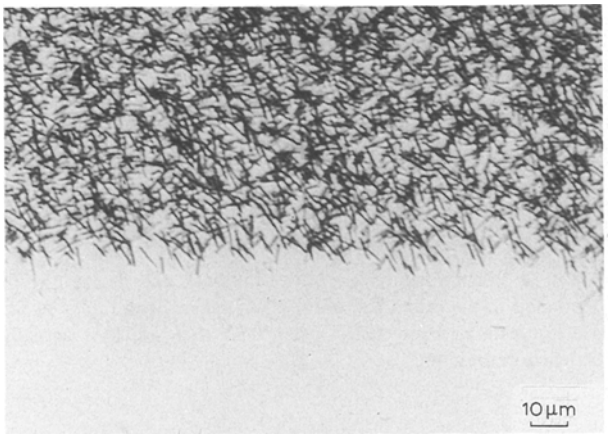

Figure 7 Etched detector shows result of the experiment shown in Fig. 6. There was good contact between the Pb and the mica detector.

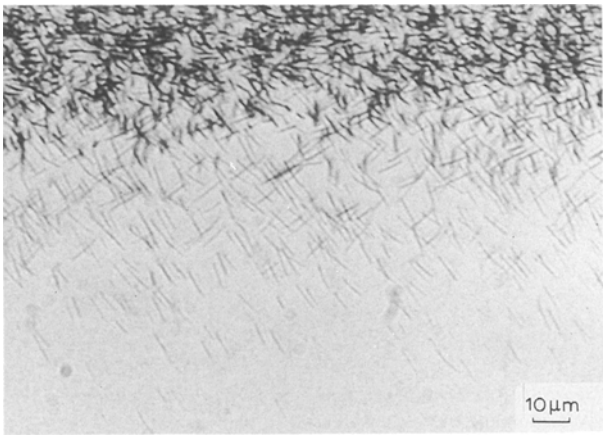

Figure 8 Etched detector from experiment shown in Fig. 6, but with space allowed between Pb and mica.

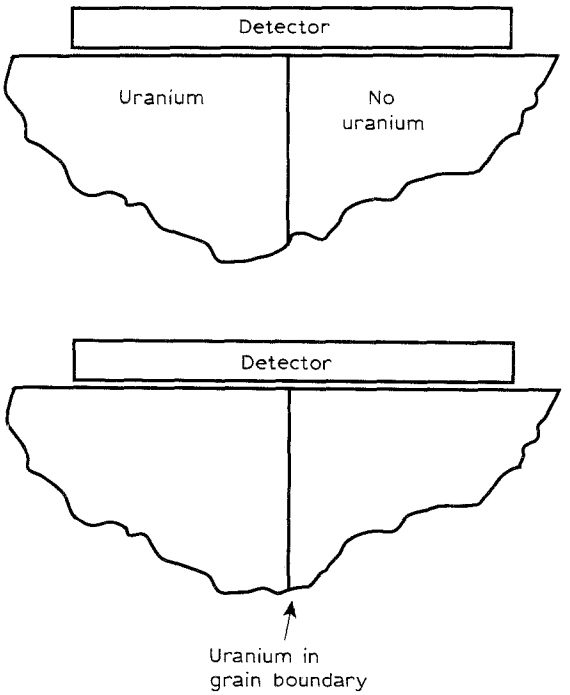

Figure 9 Two uranium distributions for which the induced fission track distributions have been modeled.

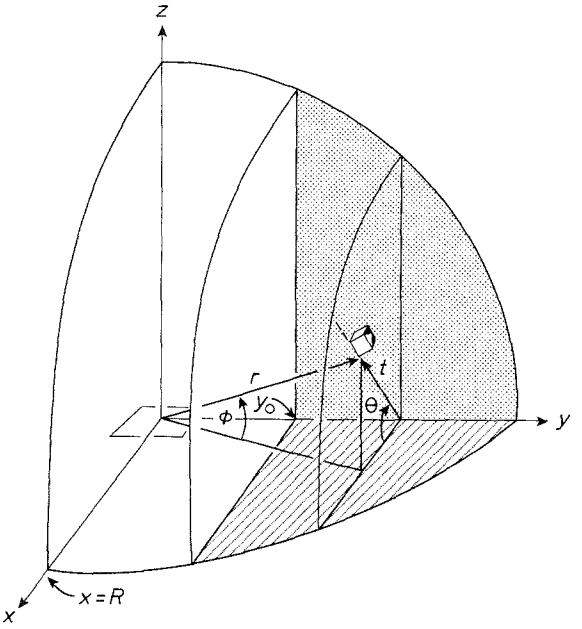

Figure 10 Coordinate system for calculating track distributions for the cases shown in Fig. 9. Uranium is in the $z > 0$ and $y > y_0$ space for the first case and for the second case it is in a plane at $y = y_0$ for $z > 0$.

resolution is marginal. One way of improving resolution is to use samples that are thin relative to the particle range.

Resolution enhancement: fission fragments that are released somewhat obliquely by uranium at depths approaching the range of fission fragments can leave tracks in the detector over a few micrometres width. This blurring can be reduced by removing the uranium at depth (i.e. thinning the sample). Figs 14 and 15 show that the track image in the detector is closer in size to the true value for thin samples. As noted earlier, producing uniformly thinned samples from originally thick samples is difficult in this range of size. Variable thickness in a sample frustrates accurate determination of the absolute value of the uranium concentration, even though it improves the detectability of abrupt spatial changes in concentration. To calculate the uranium concentration for a thin sample, i.e. of thickness $t < R$, $R/2$ in Equation 1 is replaced by $t(1 - t/2R)$.

A second way of effectively sampling uranium from a thin layer is to use a thin uniform spacer, as sketched in Fig. 16, to slow down fission fragments so that those moving obliquely toward the detector are stopped short of the detector and fail to leave tracks. If the width of the absorber is w, then to calculate the concentration of uranium, $R/2$ in Equation 1 is replaced by $[1 - w/R_s]^2/2R$, where R_s is the fission

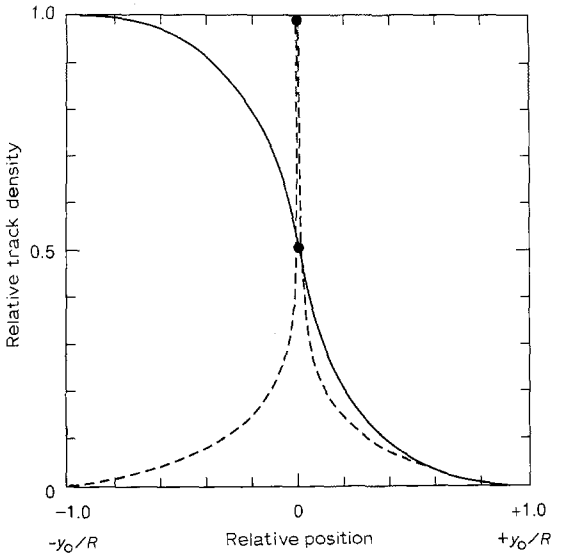

Figure 11 Track density versus position calculated for the abrupt changes shown in Fig. 9. The solid line is the uranium concentration as expected at the external surface of a crystal; the dashed line is for a planar sheet, such as would be expected if uranium were solely on grain surfaces.

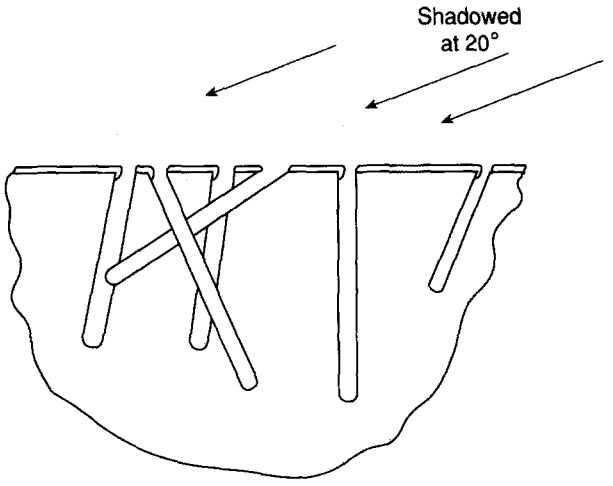

Figure 12 Shadowing technique [21] coats the detector with an opaque layer except at the holes. Transmitted light from below gives a starfield of lights on a black background.

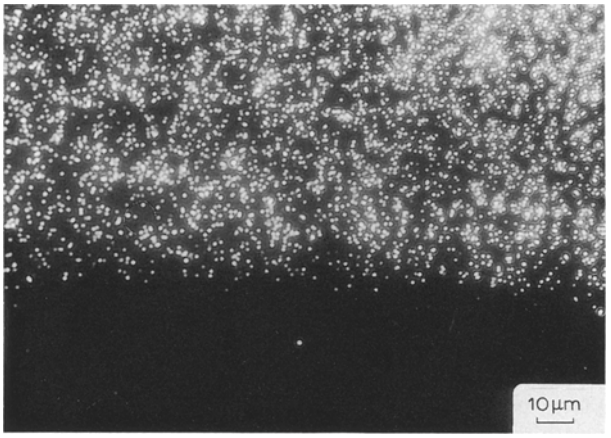

Figure 13 Shadowing technique applied to an area like that in Fig. 7.

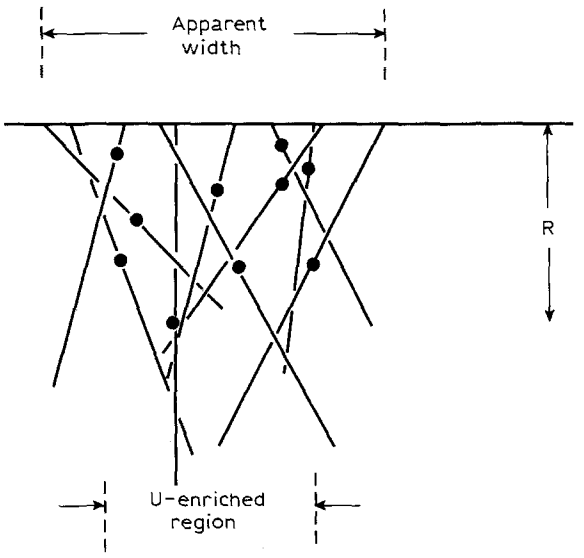

Figure 14 When fission fragments can reach the detector from depths up to the range, the width of the region with tracks in the detector can be appreciably wider than that which is actually enriched in uranium.

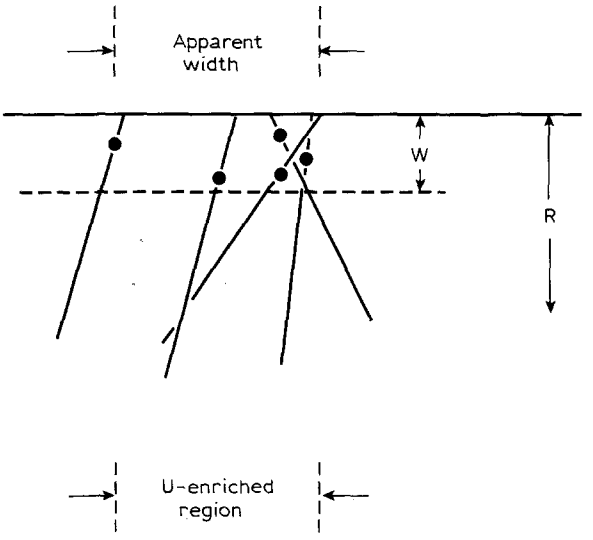

Figure 15 For a thin layer, the same sample as is shown in Fig. 13 gives an image width that is closer to the true value.

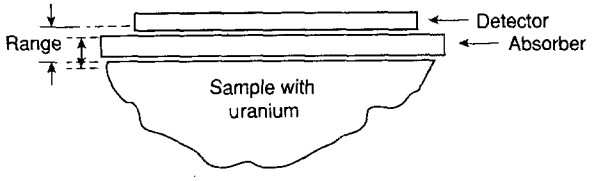

Figure 16 Absorber foil technique is designed to allow only those fission fragments that are nearly perpendicular to the detector to be registered.

fragment range in the spacer material [22]. This reduction is quadratic rather than linear (as in the preceding paragraph) because a second consideration enters. In both cases the thickness of the layer that can inject fission fragments into the detector is reduced below R. In the second case the distance of the layer from the surface is increased, and the resulting solid-angle effect produces the second factor of $1 - w/R_s$.

3. Oxide superconductors: experimental procedure

Two forms of material were tested: Y–Ba–Cu–O, with both random [10] and aligned [11, 13] crystal orientations in the form of bulk pieces, and Bi–Pb–Sr–Ca–Cu–O in both the 2212 and 2223 compositions in the form of powders [11, 12]. Grain diameters averaged $\sim 10\,\mu m$ in the bulk samples, while the powders were plates, typically $20 \times 10 \times 1\,\mu m$. Projected sizes range up to $10 \times 30\,\mu m$ and $30 \times 30\,\mu m$ for bulk and powder samples. Average fission fragment ranges are 8.1, 9.3 and 8.8 μm for Y–Ba–Cu–O, 2212 and 2223, respectively, with the effective ranges, as noted earlier being slightly less: 6.9, 7.9 and 7.5 μm.

Since in 8 μm grains the range of fission fragments allows them to cause damage throughout the volume, it is relatively unimportant where the uranium is located. However for improved future material—either of large grain size or single crystals—it is vital to know whether the doping-plus irradiation technique will be effective.

The bulk samples of Y–Ba–Cu–O were mounted on glass slides and thinned by National Petrographic, Houston, TX, to nominal thicknesses of 1 μm for random and aligned samples with nominally 380 atomic p.p.m. of uranium and 5 μm for a non-aligned 150 p.p.m. sample. The thickness could be measured microscopically at steps where occasional grains had flaked out of the mount. They gave mean values of 5.3 μm for the 150 p.p.m. sample and 3.5 μm and 3.1 μm for the other two, with significant variations across the sections. Powders were encapsulated in epoxy and then polished to reveal internal surfaces.

For irradiation the samples were mounted as shown in Fig. 17, using rubber pads plus aluminium wrapping to produce firm sample–detector contact. The bulk polycrystalline samples were mounted with 12 μm polycarbonate absorber foils. Irradiation with a nominal 2×10^{16} thermal neutrons cm^{-2} was performed at "hole PN" of the Brookhaven Medical Reactor. The actual fluence, derived from two glass fission-track dosimeters [23] was $2.14\ (\pm 0.06) \times 10^{16}$ neutrons cm^{-2}.

After return the muscovite mica detectors were etched for 10 min at 23 °C in 48% HF to produce tracks of $\sim 0.3\,\mu m$ diameter, rinsed in H_2O, soaked for 10 min at 23 °C in 12% NH_4OH to neutralize any residual acid, rinsed in distilled H_2O and then ethanol, and dried. Samples were then coated with 50 nm of Al evaporated at 20 °C to the plane of the surface, as sketched in Fig. 12. To measure uranium concentrations, track openings can be viewed directly in a microscope or photographed and counted from enlarged photos.

Electron microprobe measurements were made of uranium in Y–Ba–Cu–O. These have high spatial resolution but low sensitivity to uranium.

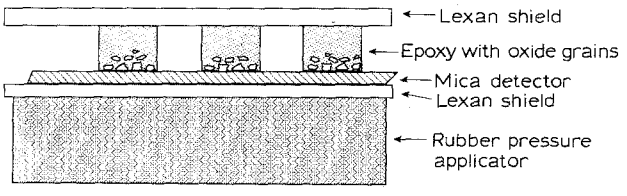

Figure 17 Sample and detector packaging used during neutron irradiation of powder samples. Al foil wrapping compresses the rubber to apply pressure between sample and detector.

4. Results

4.1. Uranium concentrations

Because of the uncertainties and variabilities in thickness of the thin sections the values of uranium concentration are not well measured—the method having optimized spatial resolution at the expense of this

TABLE I Uranium concentrations in powder samples of Bi–Pb–Sr–Ca–Cu–O (atomic parts per million)

Composition	Nominal uranium	Measured uranium
2212	0	⩽ 0.09
2212	220	160
2212	440	370
2223	0	⩽ 0.2
2223	200	110
2223	400	300

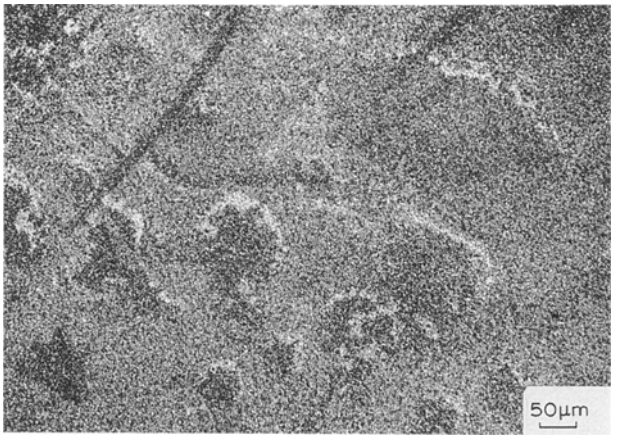

Figure 18 Fission-track map of uranium in Y–Ba–Cu–O thin section (~ 3 μm thick). At least three phases are evident and uranium concentrations are variable in the major phase (nominally 380 p.p.m. of uranium).

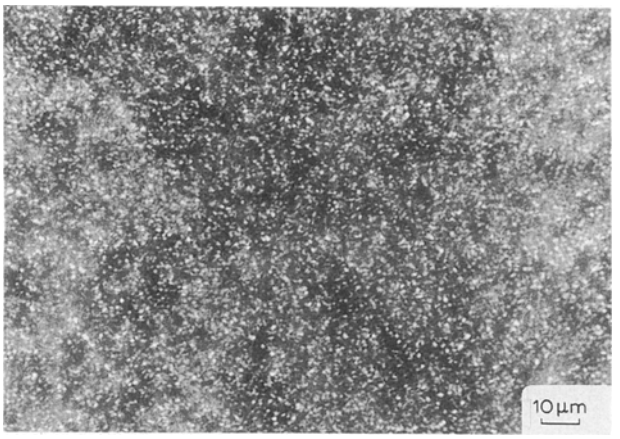

Figure 19 Uranium fission-track map at higher magnification for the same sample as in Fig. 18.

uncertainty. Estimates give 100–950 p.p.m. where the nominal design values that were used are 150 and 380 p.p.m.

For the powder samples the typical highest track counts opposite grains in the mounts were used to derive the results listed in Table I. The values are mostly slightly less than the nominal, but within what can be expected for the sizes and shapes of the powder particles.

The significance of these rough checks between design values and observed uranium concentrations is that major fractions of uranium were not lost, nor

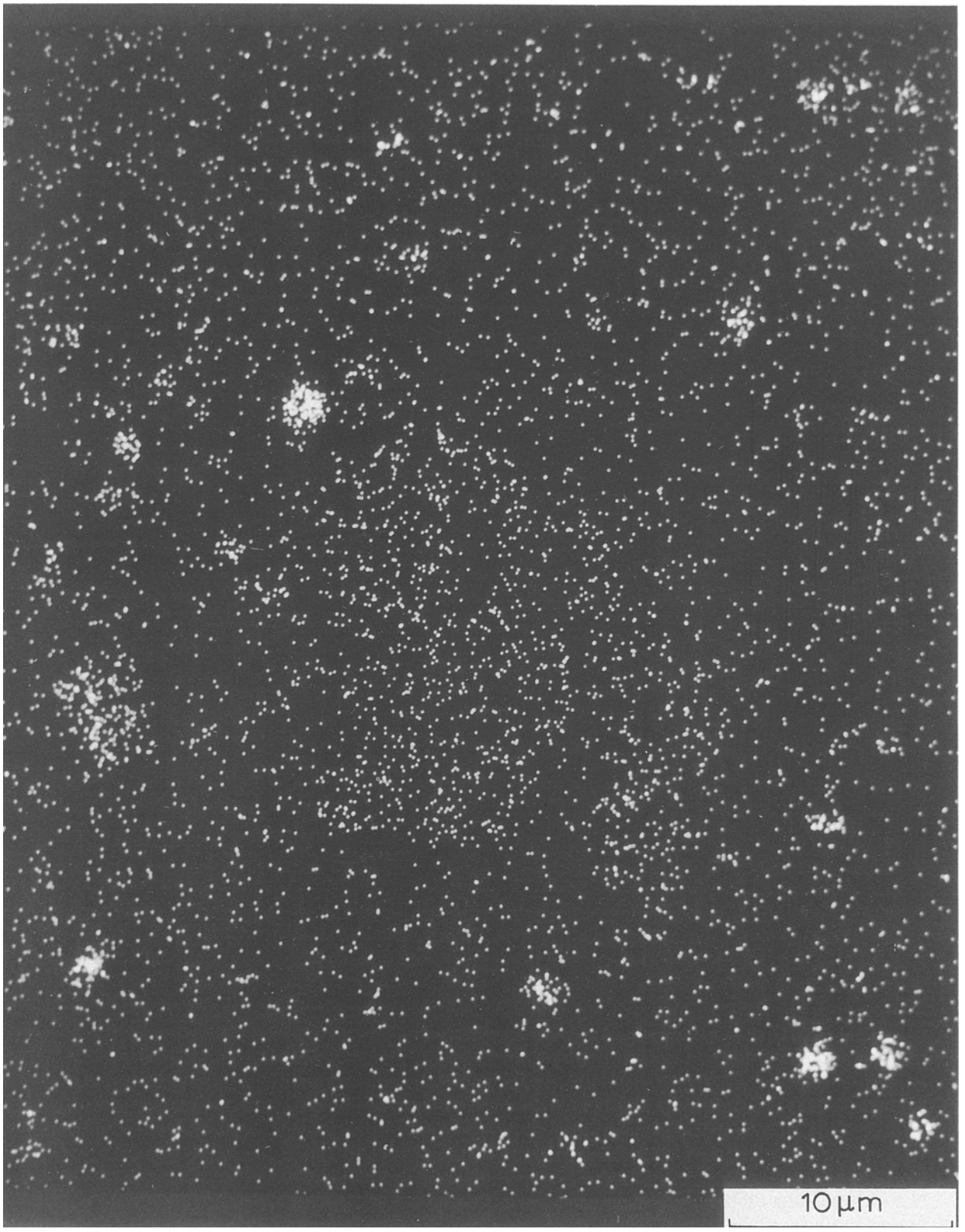

Figure 20 Microprobe image of uranium distribution in Y–Ba–Cu–O with 380 p.p.m. of uranium. The bright spots are regions with about 5 times the average uranium content. Compare to Fig. 18.

were major fractions deposited in a few minority phase particles (as can occur for example in mineral assemblages) [15].

4.2. Uranium distributions, bulk Y–Ba–Cu–O

The uranium distributions in the bulk polycrystalline samples show evidence for three or more phases, and even within the majority, superconducting phase there is non-uniformity. Figs 18 and 19 show fission track maps at low and high magnification, and Fig. 20 is an electron microprobe image of uranium in the same sample, which is Y–Ba–Cu–O with nominally 380 p.p.m. of uranium [10]. Fig. 18 is a non-typical area that was chosen to show that there are some regions with noticeably lower than average uranium content with (often) adjacent regions of higher than usual uranium. The general background level is typical of the major phase, shown also at higher magnification in Fig. 19. The electron microprobe shows a few point-like regions of high uranium (Fig. 20), but the concentration of the inclusions times their uranium content (0.2 atomic %) accounts for only a small fraction of the total uranium present. Most of the other dispersed bright dots in Fig. 20 are instrumental background. Dominantly the uranium lies in the major phase, and there is no indication of grain boundary segregation. The samples with aligned crystals made from the same 380 p.p.m. composition [11, 13] show greater non-uniformity in the superconducting phase (Fig. 21) than did the sample with random crystal orientations (Fig. 19). In contrast, variability is somewhat less in a randomly-oriented sample with reduced (125 atom p.p.m.) uranium [10], as shown in Figs 22 and 23. Again, no strong local concentrations are seen that would indicate uranium is mostly in minority phases or grain boundaries.

It may be worth noting that the relative effectiveness of uranium doping in enhancing critical current decreased in the sequence 125 p.p.m. random orientation, 380 p.p.m. random, 380 p.p.m. aligned—the order of ascending non-uniformity in uranium distributions. It is not known whether this correlation is physically significant or a statistical artifact.

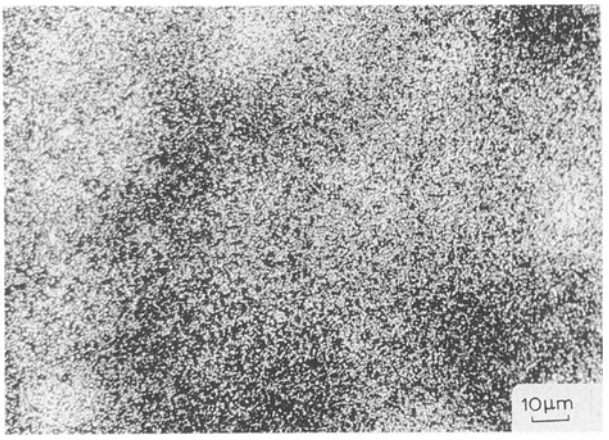

Figure 21 Fission-track uranium map in aligned Y–Ba–Cu–O with 380 p.p.m. of uranium. Greater clumping is evident than in the non-aligned material (Fig. 19).

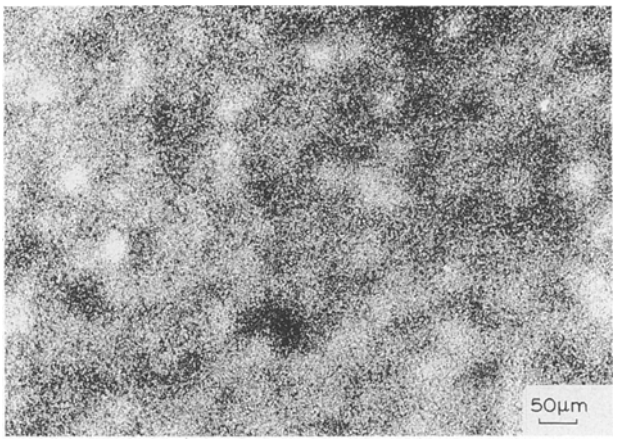

Figure 22 Uranium distribution in Y–Ba–Cu–O with 125 p.p.m. uranium.

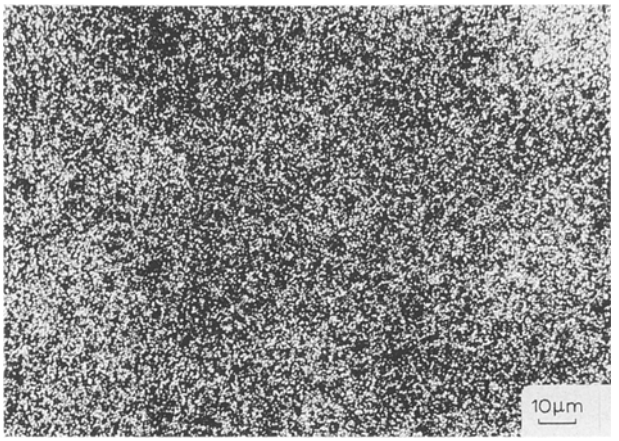

Figure 23 As in Fig. 22, but at higher magnification.

4.3. Uranium distributions, Bi–Pb–Sr–Ca–Cu–O powder

In this case, since the powder [11, 12] is embedded in a low-uranium matrix, non-uniformity is inevitable because of separation of particles. One needs to look for non-uniformity within images of individual particles. Figs 24–26 show at high and low magnification typical uranium distributions in material with 2212 composition (Figs 24 and 25) and in 2223 material (Fig. 26). In general, uranium-rich hot spots are few or absent. The small white spots with sharp edges in Fig. 24 are thought to be defects in the aluminium coating.

5. Discussion

The uranium maps of all samples were fully scanned at low magnification for uranium that was localized enough that fission fragments would have failed to reach and damage portions of the primary superconducting phases. No such significant localization was seen in any of the three Y–Ba–Cu–O samples or six Bi–Pb–Sr–Ca–Cu–O powders. It should also be emphasized, as noted earlier, that although typical grain sizes were $\sim 10\,\mu m$, larger grains up to $\sim 30\,\mu m$ were sufficiently abundant that they would

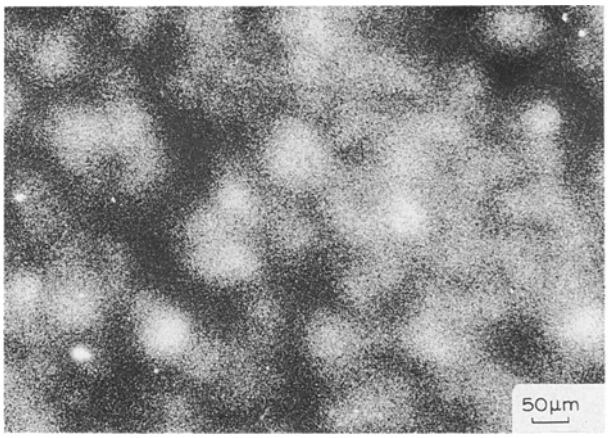

Figure 24 Uranium in 2212 Bi–Pb–Sr–Ca–Cu–O powder (400 p.p.m. uranium).

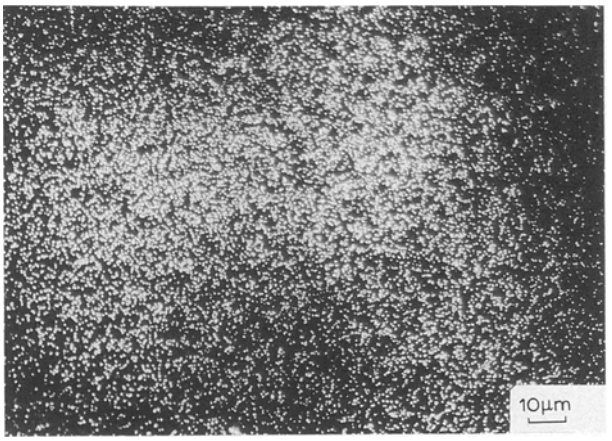

Figure 25 As in Fig. 24, but at higher magnification.

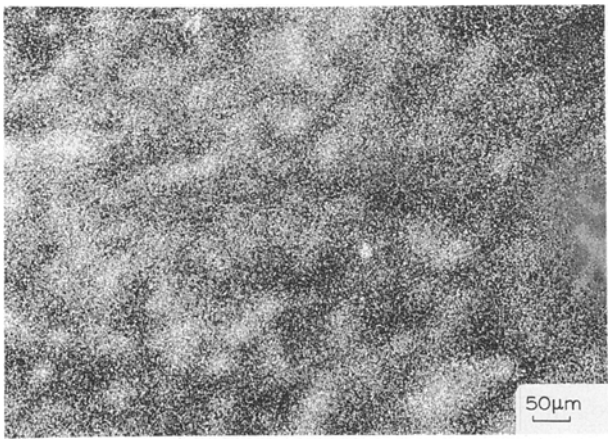

Figure 26 Uranium in 2223 Bi–Pb–Sr–Ca–Cu–O powder (400 p.p.m. uranium).

have readily shown non-uniformities had the uranium varied over that distance. Further, as described in section 2, the resolution of the technique used should have revealed changes over the abundant 10 μm grains had variations been significant. One caveat should be noted. Because the Bi–Pb–Sr–Ca–Cu–O grains were thin (~ 1–2 μm), fission fragments could readily cross individual grains. Therefore whether uranium coated the grains uniformly or was uniformly within the grains could not be decided.

6. Conclusions

The usefulness has been reviewed of nuclear track activation as a means of mapping uranium in various superconducting materials, and the limits in resolution were described. New measurements close to the resolution limits allow two conclusions:

(1) in Y–Ba–Cu–O the uranium is mostly within the superconducting phase;

(2) in Bi–Pb–Ca–Sr–O it can be said only that the uranium is not primarily in minor phases. Resolution is such that the uranium could either uniformly coat grains or lie within them.

Acknowledgements

The author is pleased to thank N. E. Holden for the neutron irradiation, A. S. Holik for microphotographic work, R. C. Margas for deposition of thin metal films, L. Peluso for electron microprobe results, and R. H. Arendt, H. R. Hart, Jr and K. W. Lay for helpful discussions.

References

1. J. P. McEVOY, Jr, R. F. DECALL and R. L. NOVAK, *Appl. Phys. Lett* **4** (1964) 43.
2. P. S. SWARTZ, H. R. HART, Jr and R. L. FLEISCHER, *ibid.* **4** (1964) 71.
3. G. W. CULLEN and R. L. NOVAK, *ibid.* **4** (1964) 147.
4. S. T. SEKULA, D. K. CHRISTEN, H. R. KERCHNER, J. R. THOMPSON, L. A. BOATNER and B. C. SALES, *Jpn. J. Appl. Phys.* **26**, Suppl. 26-3 (1987) 1185.
5. H. LUPFER, I. APFELSTEDT, W. SCHAUER, R. FLUKIGER, R. MEIER-HIRMER, H. WUHL and H. SCHEURER, *Z. Phys. B* **69** (1987) 167.
6. A. UMEZAWA, G. W. CRABTREE, J. Z. LIU, H. W. WEBER, W.K.KWOK, L.H.NUNEZ, T. J.MORAN, C. H. SOWERS and H. CLAUS, *Phys. Rev. B* **36** (1987) 7151.
7. C. P. BEAN, R. L. FLEISCHER, P. S. SWARTZ and H. R. HART, Jr, *J. Appl. Phys.* **37** (1966) 2218.
8. P. S. SCHWARTZ, H. R. HART, Jr and R. L. FLEISCHER (1966), unpublished (see Fig. 7 in [9]).
9. R. L. FLEISCHER, H. W. ALTER, S. C. FURMAN, P. B. PRICE and R. M. WALKER, *Science* **178** (1972) 255.
10. R. L. FLEISCHER, H. R. HART, K. W. LAY and F. E. LUBORSKY, *Phys. Rev. B***40** (1989) 2163.
11. F. E. LUBORSKY, R. H. ARENDT, R. L. FLEISCHER, H. R. HART, Jr, K. W. LAY, J. E. TKACZYK and D. ORSINI, *J. Mater. Res.* **6** (1991) 28.
12. H. R. HART, Jr, F. E. LUBORSKY, R. H. ARENDT, R. L. FLEISCHER, K. W. LAY, J. E. TKACZYK and D. ORSINI. *IEEE Trans. Magn.* **27** (1991) 1375.
13. F. E. LUBORSKY, R. H. ARENDT, R. L. FLEISCHER, H. R. HART, Jr, K. W. LAY, J. E. TKACZYK and D. A. ORSINI, *J. Appl. Phys.* **70** (1991) 5756.
14. R. L. FLEISCHER and P. B. PRICE, *J. Geophys. Res.* **69** (1964) 331.
15. R. L. FLEISCHER, C. W. NAESER, P. B. PRICE, R. M. WALKER and U. B. MARVIN, *Science* **148** (1965) 629.
16. R. L. FLEISCHER, P. B. PRICE and R. M. WALKER, in "Nuclear Tracks in Solids" (University of California Press, Berkeley, CA, 1975).

17. P. B. PRICE and R. M. WALKER, *Appl. Phys. Lett.* **2** (1963) 23.
18. R. L. FLEISCHER, P. B. PRICE, R. M. WALKER and E. L. HUBBARD, *Phys. Rev.* **133A** (1964) 1443.
19. P. B. PRICE, R. L. FLEISCHER and C. D. MOAK, *Phys. Rev.* **167** (1968) 277.
20. R. L. FLEISCHER and O. G. RAABE, *Health Phys.* **32** (1977) 253.
21. M. G. SEITZ, R. M. WALKER and B. S. CARPENTER, *J. Appl. Phys.* **44** (1973) 510.
22. R. L. FLEISCHER, *Geochim. Cosmochim. Acta* **32** (1968) 989.
23. R. L. FLEISCHER, P. B. PRICE and R. M. WALKER, *Nucl. Sci. Engng* **22** (1965) 153.

Received 25 November
and accepted 8 December 1992